

Loop effects and non-decoupling property of SUSY QCD in $gb \rightarrow tH^-$

Guangping Gao ^{a,b}, Gongru Lu ^a, Zhaohua Xiong ^{b,c} and Jin Min Yang ^b

^a *Physics Department, Henan Normal University, Xinxiang 453002, China*

^b *Institute of Theoretical Physics, Academia Sinica, Beijing 100080, China*

^c *Institute of High Energy Physics, Academia Sinica, Beijing 100039, China*

(October 25, 2018)

One-loop SUSY QCD radiative correction to $gb \rightarrow tH^-$ cross section is calculated in the Minimal Supersymmetric Standard Model. We found that SUSY QCD is non-decoupling if the gluino mass and the parameter μ , A_t or A_b are at the same order and get large. The non-decoupling contribution can be enhanced by large $\tan\beta$ and therefore large corrections to the hadronic production rates at the Tevatron and LHC are expected in the large $\tan\beta$ limit. The fundamental reason for such non-decoupling behavior is found to be some couplings in the loops being proportional to SUSY mass parameters.

14.80.Cp, 13.85.Qk, 12.60.Jv

I. INTRODUCTION

Although the Standard Model (SM) is phenomenologically successful, it is arguably an effective theory and new physics must exist at high energy scales. Among all elementary particles predicted by the SM, top quark and Higgs boson may hold the key to new physics since they are most related to the electroweak symmetry breaking. An intensive study of the properties of top quark and Higgs boson will be one of the primary tasks of particle physics in the new millennium.

So far the most intensively studied new physics model is the Minimal Supersymmetric Standard Model (MSSM) [1]. This model predicts the existence of five Higgs bosons, H^0 , h^0 , A^0 and H^\pm , all of which couples to top quark. Compared to the couplings in the SM, the coupling tbH^- is an utterly new coupling. Studies [2] show that this coupling is sensitive to quantum corrections and may be a good probe of the MSSM. Although this coupling could be measured from top quark decay process $t \rightarrow H^+b$ if the charged Higgs is sufficiently light, the direct production of a top quark associated with the charged Higgs boson through the subprocess $gb \rightarrow tH^-$ at hadron colliders will be a good probe for tbH^- coupling [3]. In this work we calculate the one-loop SUSY QCD corrections to this process owing to the following motivations. Firstly, if the charged Higgs boson is heavy, $m_{H^\pm} > m_t + m_b$, as a main charged Higgs production channel [5], the process $gb \rightarrow tH^-$ will provide sizable cross section at the Tevatron and LHC. The supersymmetric radiative corrections, especially the SUSY-QCD corrections, to this high energy process may be significant, as was found for other similar processes [6–10]. Secondly, some recent studies [8–10] showed that SUSY-QCD may be non-decoupling in some processes involving Higgs bosons. As is well known, the decoupling theorem [11] states that under certain conditions in a given quantum field theory with light and heavy particles, if the heavy particles are integrated out to all orders in perturbation theory, the remaining effective action to be valid at energies much lower than the heavy particle masses does not show any trace of these heavy particles. If SUSY QCD is non-decoupling in some cases, we need a proper understanding and thus we need to further investigate such non-decoupling property of SUSY QCD. $gb \rightarrow tH^-$ will be an ideal process for this purpose.

This paper is organized as follows. In Section II we present the formula for the one-loop SUSY-QCD corrections to the $gb \rightarrow tH^\pm$ process. In Section III we scan the parameter space of MSSM to estimate the size of SUSY-QCD corrections. In Section IV we study the decoupling behavior of SUSY QCD. A discussion on how the decoupling and non-decoupling take place is also given. Finally, the conclusions are summarized in Section V.

II. CALCULATIONS

The subprocess $gb \rightarrow tH^-$ occurs through both s-channel and t-channel. The tree-level amplitude is given by

$$M_0 = M_0^{(s)} + M_0^{(t)}, \quad (2.1)$$

where $M_0^{(s)}$ and $M_0^{(t)}$ represent the amplitudes arising from the s-channel diagram shown in Fig. 1(a) and the t-channel diagram shown in Fig. 1(b), respectively. Their amplitudes can be expressed as

$$M_0^{(s)} = \frac{igg_s V_{tb}}{\sqrt{2}m_W(\hat{s} - m_b^2)} \bar{u}(p_t) [2\eta_t p_b^\mu P_L + 2\eta_b p_b^\mu P_R - \eta_t \gamma^\mu \not{k} P_L - \eta_b \gamma^\mu \not{k} P_R] u(p_b) \varepsilon_\mu(k) T_{ij}^a, \quad (2.2)$$

$$M_0^{(t)} = \frac{igg_s V_{tb}}{\sqrt{2}m_W(\hat{t} - m_t^2)} \bar{u}(p_t) [2\eta_t p_t^\mu P_L + 2\eta_b p_t^\mu P_R - \eta_t \gamma^\mu \not{k} P_L - \eta_b \gamma^\mu \not{k} P_R] u(p_b) \varepsilon_\mu(k) T_{ij}^a, \quad (2.3)$$

where $P_{R,L} \equiv (1 \pm \gamma_5)/2$, and p_t , p_b and k are the momenta of the outgoing top quark, the incoming bottom quark and the incoming gluon, respectively. \hat{s} and \hat{t} are the subprocess Mandelstam variables defined by $\hat{s} = (p_b + k)^2 = (p_t + p_{H^-})^2$ and $\hat{t} = (p_t - k)^2 = (p_{H^-} - p_b)^2$. T^a are the $SU(3)$ color matrices and $\tan \beta = v_2/v_1$ is the ratio of the vacuum expectation values of the two Higgs doublets. The constants $\eta_{b,t}$ are defined by $\eta_b = m_b \tan \beta$ and $\eta_t = m_t \cot \beta$.

The one-loop Feynman diagrams of SUSY QCD corrections are shown in Fig. 1(c)-(o). In our calculations we use dimensional regularization to control all the ultraviolet divergences in the virtual loop corrections and we adopt the on-mass-shell renormalization scheme. The renormalization condition for the coupling constant g_s is similar to that for the coupling constant e in QED, i.e., the coupling of the photon (gluon) to a pair of fermions is required to recover the tree-level result in the limit of zero momentum transfer. This condition yields

$$\frac{\delta g_s}{g_s} = -\frac{1}{2} \delta Z_2^g, \quad (2.4)$$

where δg_s and Z_2^g are the renormalization constants defined by $g_s^0 \equiv g_s + \delta g_s$ and $A_\mu^0 \equiv \sqrt{Z_2^g} A_\mu$ with g_s^0 denoting bare coupling constant and A_μ^0 bare gluon fields (color index suppressed).

Including the one-loop SUSY QCD corrections, the renormalized amplitude for $gb \rightarrow tH^-$ can be written as

$$M_{ren} = M_0^{(s)} + M_0^{(t)} + \delta M, \quad (2.5)$$

where δM represents the one-loop SUSY QCD corrections given by

$$\delta M = \delta M^{V_1(s)} + \delta M^{V_2(s)} + \delta M^{s(s)} + \delta M^{box} + \delta M^{V_1(t)} + \delta M^{V_2(t)} + \delta M^{s(t)}. \quad (2.6)$$

Here $\delta M^{V_1(s)}$, $\delta M^{V_2(s)}$ and $\delta M^{s(s)}$ represent the renormalized vertex $gb\bar{b}$, $t\bar{b}H^-$ and the renormalized propagator in the s-channel diagram, respectively. Similar definitions are for $\delta M^{V_1(t)}$, $\delta M^{V_2(t)}$ and $\delta M^{s(t)}$ in the t-channel diagram. The contribution of the box diagram is denoted by δM^{box} . Each δM^l can be decomposed as

$$\begin{aligned} \delta M^l = & \frac{igg_s^3 T_{ij}^a V_{tb}}{16\sqrt{2}\pi^2 m_W} C^l \bar{u}(p_t) \{ F_1^l \gamma^\mu P_L + F_2^l \gamma^\mu P_R + F_3^l p_b^\mu P_L + F_4^l p_b^\mu P_R + F_5^l p_t^\mu P_L + F_6^l p_t^\mu P_R \\ & + F_7^l \gamma^\mu \not{k} P_L + F_8^l \gamma^\mu \not{k} P_R + F_9^l p_b^\mu \not{k} P_L + F_{10}^l p_b^\mu \not{k} P_R + F_{11}^l p_t^\mu \not{k} P_L + F_{12}^l p_t^\mu \not{k} P_R \} u(p_b) \varepsilon_\mu(k), \end{aligned} \quad (2.7)$$

where the coefficients C^l and the form factors F_n^l are given explicitly in Appendix A and B, respectively. We have checked that all the ultraviolet divergences canceled as a result of renormalizability of MSSM.

The amplitude squared is given by

$$\overline{\sum} |M_{ren}|^2 = \overline{\sum} \left| M_0^{(s)} + M_0^{(t)} \right|^2 + 2Re \overline{\sum} \left[\left(M_0^{(s)} + M_0^{(t)} \right)^\dagger \delta M \right], \quad (2.8)$$

where

$$\begin{aligned} \overline{\sum} \left| M_0^{(s)} + M_0^{(t)} \right|^2 = & \frac{2g^2 g_s^2 |V_{tb}|^2}{N_C m_W^2} \left\{ \frac{1}{(\hat{s} - m_b^2)^2} [(\eta_b^2 + \eta_t^2)(p_b \cdot kp_t \cdot k + 2p_b \cdot kp_b \cdot p_t - m_b^2 p_t \cdot kp_t - m_b^2 p_b \cdot p_t) \right. \\ & + 2m_b^2 m_t^2 (p_b \cdot k - m_b^2)] + \frac{1}{(\hat{t} - m_t^2)^2} [(\eta_b^2 + \eta_t^2)(p_b \cdot kp_t \cdot k + m_t^2 p_b \cdot k - m_t^2 p_b \cdot p_t) \\ & + 2m_b^2 m_t^2 (p_t \cdot k - m_t^2)] + \frac{1}{(\hat{s} - m_b^2)(\hat{t} - m_t^2)} [(\eta_b^2 + \eta_t^2)(2p_b \cdot kp_t \cdot k + 2p_b \cdot kp_b \cdot p_t \\ & \left. - 2(p_b \cdot p_t)^2 - m_b^2 p_t \cdot k + m_t^2 p_b \cdot k) + 2m_b^2 m_t^2 (p_t \cdot k - p_b \cdot k - 2p_b \cdot p_t)] \right\}, \end{aligned} \quad (2.9)$$

$$\overline{\sum} \left(M_0^{(s)} + M_0^{(t)} \right)^\dagger \delta M = -\frac{g^2 g_s^4 |V_{tb}|^2}{64 N_C \pi^2 m_W^2} \sum_{n=1}^{12} \left[\frac{1}{\hat{s} - m_b^2} h_n^{(s)} + \frac{1}{\hat{t} - m_t^2} h_n^{(t)} \right] C^l F_n^l. \quad (2.10)$$

Here the color factor $N_C = 3$, and $h_n^{(s)}$ and $h_n^{(t)}$ can be found in Appendix A.

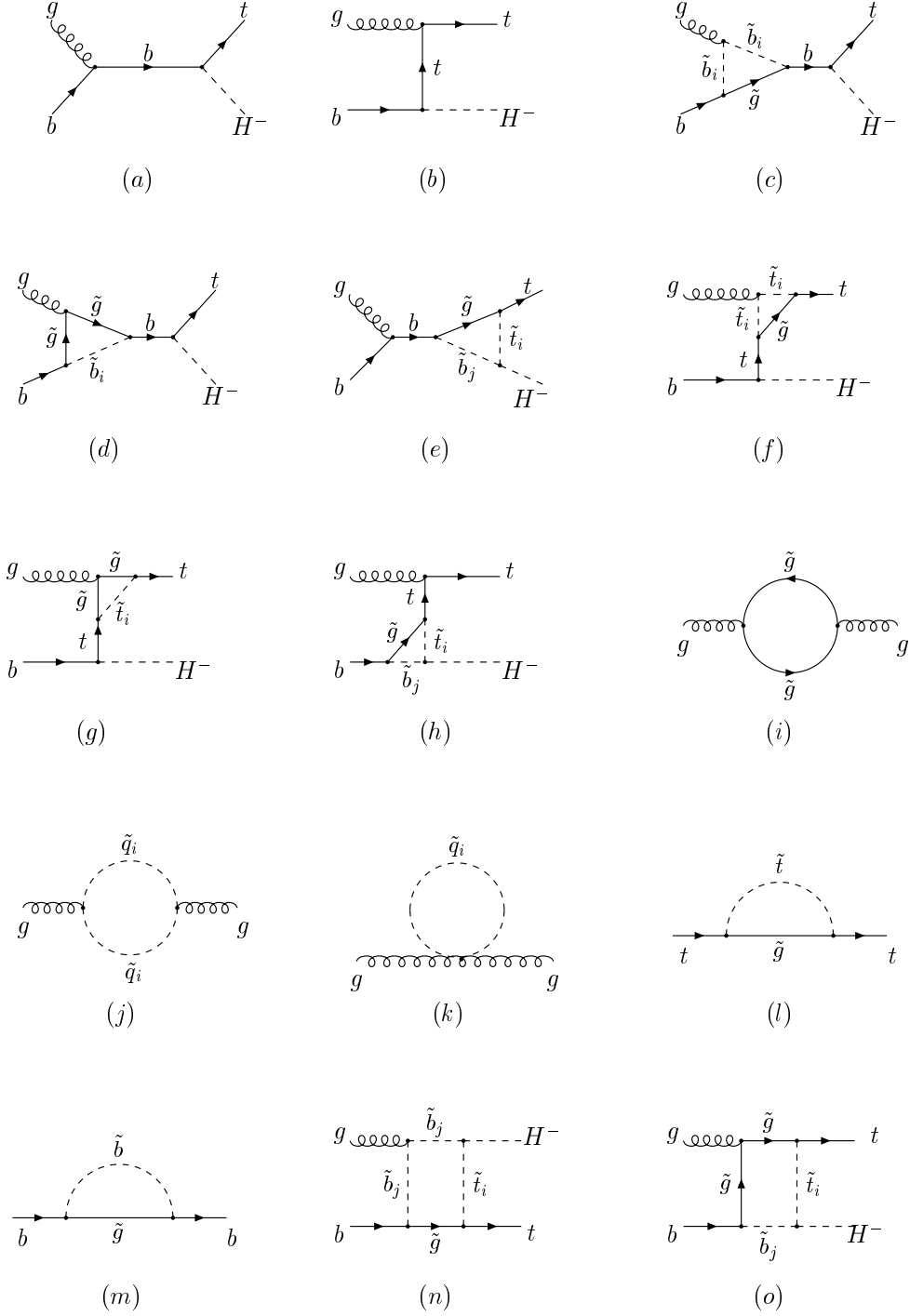


FIG. 1. Feynman diagrams of $gb \rightarrow tH^-$ with one-loop SUSY QCD corrections: (a) and (b) are tree level diagrams ; (c) – (e) are one-loop vertex diagrams for s-channel ; (f) – (h) are one-loop vertex diagrams for t-channel ; (i) – (m) are self-energy diagrams; (n, o) are the box diagrams.

The cross section for the parton process $gb \rightarrow tH^-$ is

$$\hat{\sigma}(\hat{s}) = \int_{\hat{t}_{min}}^{\hat{t}_{max}} \frac{1}{16\pi\hat{s}^2} \overline{\Sigma} |M_{ren}|^2 d\hat{t}, \quad (2.11)$$

with

$$\hat{t}_{max,min} = \frac{1}{2} \left\{ m_t^2 + m_{H^-}^2 - \hat{s} \pm \sqrt{[\hat{s} - (m_t + m_{H^-})^2][\hat{s} - (m_t - m_{H^-})^2]} \right\}. \quad (2.12)$$

The total hadronic cross section for $pp(\text{or } p\bar{p}) \rightarrow tH^- + X$ can be obtained by folding the subprocess cross section $\hat{\sigma}$ with the parton luminosity

$$\sigma(s) = \int_{\tau_0}^1 d\tau \frac{dL}{d\tau} \hat{\sigma}(\hat{s} = s\tau), \quad (2.13)$$

where $\tau_0 = (m_t + m_{H^-})^2/s$, and s is the $pp(\text{or } p\bar{p})$ center-of-mass energy squared. $dL/d\tau$ is the parton luminosity given by

$$\frac{dL}{d\tau} = \int_x^1 \frac{dx}{x} [f_g^p(x, Q) f_b^p(\tau/x, Q) + (g \leftrightarrow b)], \quad (2.14)$$

where f_b^p and f_g^p are the bottom quark and gluon distribution functions in a proton, respectively. In our numerical calculation, we use the CTEQ5L parton distribution functions [12] with $Q = m_t + m_{H^-}$.

To show the size of the corrections, we define the relative quantity as

$$\Delta_{SQCD} = \frac{\sigma - \sigma_0}{\sigma_0}, \quad (2.15)$$

where σ_0 is the tree-level cross section.

III. NUMERICAL RESULTS

Before performing numerical calculations, we take a look at the relevant parameters involved.

For the SM parameters, we took $m_W = 80.448$ GeV, $m_Z = 91.187$ GeV, $m_t = 176$ GeV, $m_b = 4.5$ GeV, and used the two-loop running coupling constant $\alpha_s(Q)$.

For the SUSY parameters, apart from the charged Higgs mass, gluino mass and $\tan\beta$, the mass parameters of stops and sbottoms are involved. The mass square matrices of stop and sbottoms take the form ($q = t$ or b) [13]

$$M_{\tilde{q}}^2 = \begin{pmatrix} m_{\tilde{q}_L}^2 & m_q X_q^\dagger \\ m_q X_q & m_{\tilde{q}_R}^2 \end{pmatrix}, \quad (3.1)$$

where

$$\begin{aligned} m_{\tilde{q}_L}^2 &= m_{\tilde{Q}}^2 + m_q^2 - m_Z^2 \left(\frac{1}{2} + e_q \sin^2 \theta_W \right) \cos(2\beta), \\ m_{\tilde{q}_R}^2 &= m_{\tilde{U}, \tilde{D}}^2 + m_q^2 + e_q m_Z^2 \sin^2 \theta_W \cos(2\beta), \\ X_q &= \begin{cases} A_t - \mu \cot \beta, & \text{for } q = t, \\ A_b - \mu \tan \beta, & \text{for } q = b. \end{cases} \end{aligned} \quad (3.2)$$

Here $m_{\tilde{Q}}^2$, $m_{\tilde{U}}$ and $m_{\tilde{D}}^2$ are soft-breaking mass terms for left-handed squark doublet \tilde{Q} , right-handed up squark \tilde{U} and down squark \tilde{D} , respectively. $A_b(A_t)$ is the coefficient of the trilinear term $H_1 \tilde{Q} \tilde{D}$ ($H_2 \tilde{Q} \tilde{U}$) in soft-breaking terms and μ the bilinear coupling of the two Higgs doublet in the superpotential. Thus the SUSY parameters involved in stop and sbottom mass matrices are

$$m_{\tilde{Q}}, m_{\tilde{U}}, m_{\tilde{D}}, A_t, A_b, \mu, \tan \beta.$$

The mass square matrices are diagonalized by unitary rotations ($q = t$ or b)

$$R^q = \begin{pmatrix} \cos \theta_q & \sin \theta_q \\ -\sin \theta_q & \cos \theta_q \end{pmatrix} \quad (3.3)$$

which relates the weak-eigenstates (\tilde{q}_L, \tilde{q}_R) to the mass eigenstates (\tilde{q}_1, \tilde{q}_2). Then the stop and sbottom masses as well as the mixing angles are obtained by

$$m_{\tilde{q}_{1,2}} = \frac{1}{2} \left[m_{\tilde{q}_L}^2 + m_{\tilde{q}_R}^2 \pm \sqrt{(m_{\tilde{q}_L}^2 - m_{\tilde{q}_R}^2)^2 + 4m_q^2 X_q^2} \right],$$

$$\tan 2\theta_q = \frac{2m_q X_q}{m_{\tilde{q}_L}^2 - m_{\tilde{q}_R}^2}. \quad (3.4)$$

To determinate the mixing angles completely, we adopt the convention in [14] which sets $\theta_q = \pi/4$ if $m_{\tilde{q}_L} = m_{\tilde{q}_R}$ and shifts $\pi/2$ to θ_q if $m_{\tilde{q}_L} > m_{\tilde{q}_R}$. Thus θ_q lies in the range $-\frac{\pi}{4} \leq \theta_q \leq \frac{3}{4}\pi$.

To find out the size of the one-loop SUSY QCD effects, we performed a scan over the nine-dimensional parameter space: $m_{\tilde{Q}}, m_{\tilde{U}}, m_{\tilde{D}}, A_t, A_b, \mu, \tan\beta, m_{H^-}, m_{\tilde{g}}$. In scanning we restricted m_{H^-}, A_t, A_b and μ to the sub-TeV region and required $m_{H^-} > 150$ GeV. Other mass parameters are assumed to be smaller than 5 TeV. In addition, we consider the following experimental constraints:

- (1) $\mu > 0$ and a large $\tan\beta$ in the range $5 \leq \tan\beta \leq 50$, which might be favored by the recent muon $g - 2$ measurement [15].
- (2) The LEP and CDF lower mass bounds on gluino, stop and sbottom [16]

$$m_{\tilde{t}_1} \geq 86.4 \text{ GeV}, m_{\tilde{b}_1} \geq 75.0 \text{ GeV}, m_{\tilde{g}} \geq 190 \text{ GeV}. \quad (3.5)$$

The scan results are plotted in the plane of Δ_{SQCD} versus θ_b in Fig. 2.

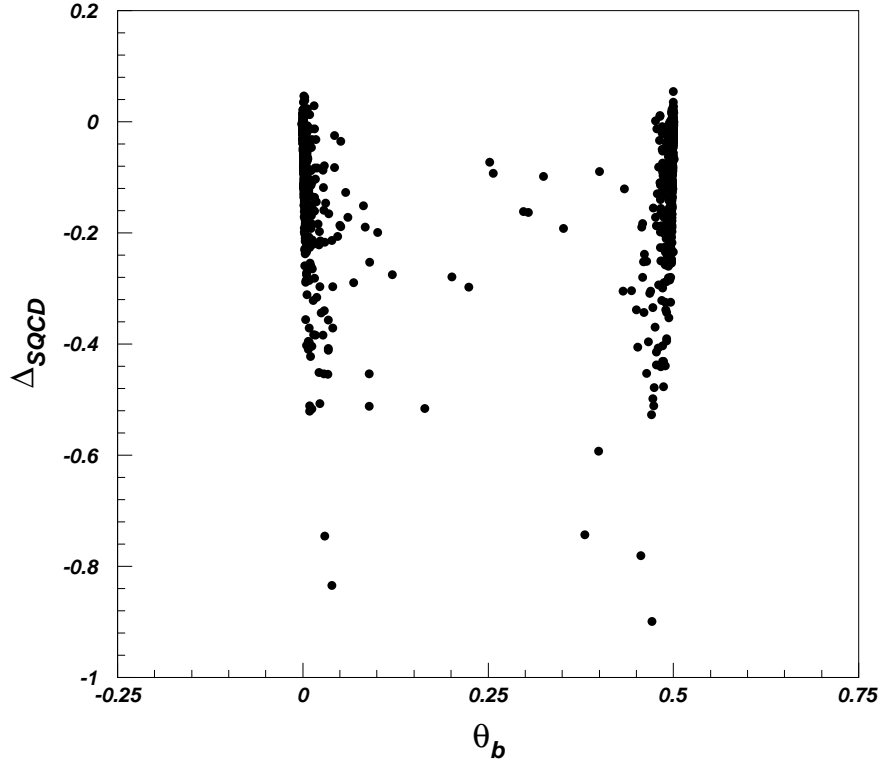


FIG. 2. The scatter plot in the plane of Δ_{SQCD} versus θ_b . The scan was performed over nine SUSY parameters. θ_b is in unit of π .

From Fig. 2 one can see that in most parameter space the mixing of sbottoms is small while the one-loop SUSY QCD effect can be quite large. In some part of the parameter space, the correction size can be larger than 20% which cannot be neglected in the study of this process at LHC.

IV. DECOUPLING PROPERTY OF SUSY QCD

To find out if SUSY QCD is decoupling from the process $gb \rightarrow tH^-$ in the large limit of SUSY mass parameters, we fix the charged Higgs mass as $m_{H^-} = 250 \text{ GeV}$ and consider the following scenarios.

(1) *Scenario A*: All squark (collectively denoted by m_S), gluino masses and μ or A parameters are of the same size and much heavier than the electroweak scale, i.e.,

$$m_S \sim m_{\tilde{Q}} \sim m_{\tilde{U}} \sim m_{\tilde{D}} \sim m_{\tilde{g}} \sim \mu \text{ or } A_t \text{ or } A_b \sim m_S \gg M_{EW} \quad (4.1)$$

In this case, both mixings in the sbottom and stop sectors reach their maximal values, i.e., $\theta_t \sim \pm \frac{\pi}{4}$, $\theta_b \sim \pm \frac{\pi}{4}$. As shown in Eqs. (6.3-6.5), the couplings α_{ij} in the vertex $H^- \tilde{t}_i \tilde{b}_j$ are proportional to the linear combination of $\mu + A_b \tan \beta$ and $\mu + A_t \cot \beta$. Considering that the couplings α_{ij} are proportional to m_S as μ or $A_{t,b}$ gets large as m_S , and the loop scalar integral functions C_0 goes to $-1/2m_S^2$ as $m_S \gg \hat{s}$ (see Eq. (6.18) and Eq. (B8) in Ref. [9]), one can infer that the terms $\alpha_{ij} A_{ij}^{2(L,R)} C_0^6 m_{\tilde{g}}$ which arise from the vertex correction to $H^- tb$ do not vanish but go to a non-zero constant, showing a clear indication of *non-decoupling* behavior. In fact, such non-decoupling behavior will happen as long as the gluino mass and μ or A parameters are of the same order, not necessarily degenerate. Actually, from the expansions of the three- and four-point loop integrals in the asymptotic large mass limit in Appendix C, one can see this fact.

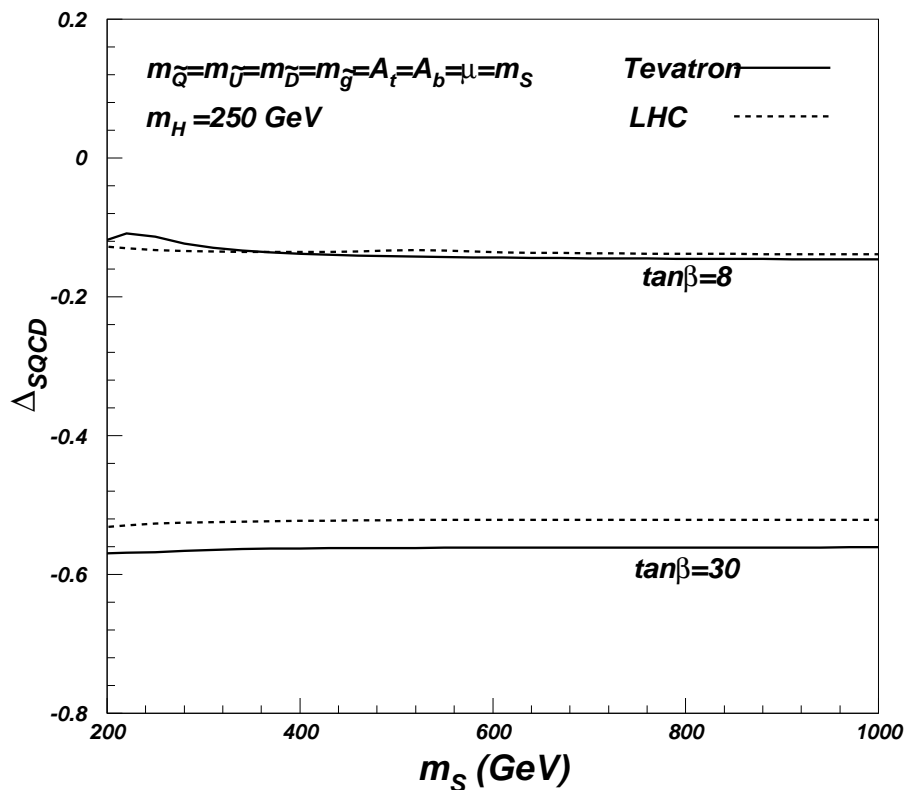


FIG. 3. Non-decoupling behavior of Δ_{SQCD} with $m_{\tilde{Q}} = m_{\tilde{U}} = m_{\tilde{D}} = m_{\tilde{g}} = A_b = A_t = \mu = m_S$ and for different values of $\tan \beta$. Corrections at the Tevatron with $\sqrt{s} = 2 \text{ TeV}$ (solid lines) and at the LHC $\sqrt{s} = 14 \text{ TeV}$ (dashed lines) are plotted respectively.

As illustrative examples, we plot the dependence of the SUSY-QCD correction to $gb \rightarrow tH^-$ on the common SUSY parameter m_S in Fig. 3. From this figure one can see that the non-decoupling behavior indeed happens. As for the dependence of the non-decoupling effects on $\tan \beta$, it is quite involved and complicated. For the parameter values chosen in our numerical examples, the corrections are enhanced by $\tan \beta$.

(2) *Scenario B*: The gluino mass and μ are of the same order (collectively denoted by m_S) and get much larger than squark masses and electroweak scale, i.e.,

$$\sim m_{\tilde{g}} \sim \mu \gg m_S \sim m_{\tilde{Q}} \sim m_{\tilde{U}} \sim m_{\tilde{D}} \geq M_{EW} \quad (4.2)$$

To keep stop and sbottom masses from getting large, we can set $A_t \simeq \mu \cot \beta$, $A_b \simeq \mu \tan \beta$. In this scenario, no mixings occur in the sbottom and stop sectors. Apart from the vertex correction discussed in *Scenario A*, the terms such as $\alpha_{ij} A_{ij}^{2(L,R)} D_0^2 m_{\tilde{g}}$ in the box contribution (see Eq. (6.12) and (6.24)) do not vanish either since the four-point integral functions $D_{(0,1l)}^2 \rightarrow 1/m_{\tilde{g}}^2$ ($l = 1, 2, 3$) when $m_{\tilde{g}}^2 \gg \hat{s}$. So in this case the SUSY QCD is non-decoupling. This differs from *Scenario A* where $D_{(0,1l)} \rightarrow 1/m_{\tilde{g}}^4$.

Although the non-decoupling effects can arise from more diagrams in this case, the reason is the same as in Scenario A, i.e., the couplings $H^- \tilde{t}_i \tilde{b}_j$ are proportional to μ . To prove this point fully, now let's focus our attention on the terms arising from the corrections to the $g\tilde{b}\tilde{b}$ and $g\tilde{g}\tilde{g}$ vertices which are also likely to give the contributions to non-decoupling effects in both scenarios we discussed. Firstly, for example we consider the term

$$-\frac{2}{3}\eta_t C_{24}^1 - 3\eta_t [m_{\tilde{g}}^2 C_0^2 - 2C_{24}^2 + 1/2] + \frac{16\pi^2}{g_s^2} \eta_t 2\delta Z_R^b \quad (4.3)$$

in $F_3^{1(s)}$. From Eq. (6.13), (6.16), (6.18), (6.19), (6.21) and (6.22), we draw a conclusion that the term indeed cancels out. Further, it is easy to find that all terms related with $A_{\tilde{b}_i}^2$ are zero in the asymptotic large mass limit. This is also valid in the *Scenario C* and *Scenario D* we will study. Secondly, we exam the terms such as $\alpha_{ij} A_{ij}^{1(L,R)} D_0^1 m_{\tilde{g}}^2$ in Eq. (6.12). The asymptotic form of the function D_0^1 in large mass limit is always proportional to $\frac{1}{m_{\tilde{g}}^4}$ and different from D_0^2 which is proportional to $\frac{1}{m_{\tilde{g}}^2}$ in the *Scenario B*. So the terms don't cause non-decoupling either.

(3) *Scenario C*: Only the gluino mass is very large than other SUSY parameters and the electroweak scale

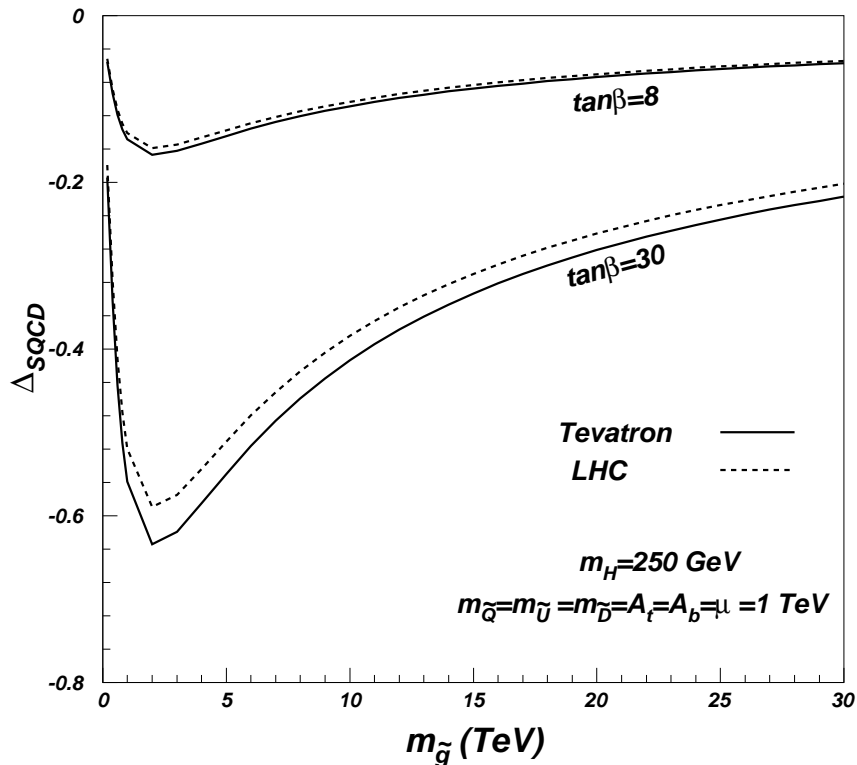


FIG. 4. Behavior of Δ_{SQCD} in the large $m_{\tilde{g}}$ limit with fixed $m_{\tilde{Q}} = m_{\tilde{U}} = m_{\tilde{D}} = A_b = A_t = \mu = 1$ TeV and for different values of $\tan \beta$. The solid and dashed lines correspond to corrections at the Tevatron with $\sqrt{s} = 2$ TeV and at the LHC $\sqrt{s} = 14$ TeV, respectively.

In this scenario, to simplify the calculation we assumed $m_S = m_{\tilde{Q}} = m_{\tilde{U}} = m_{\tilde{D}} = \mu = A_t = A_b = 1$ TeV. As shown in Fig. 4, the SUSY-QCD decouples. The reason is the couplings α_{ij} in the vertex $H^- \tilde{t}_i \tilde{b}_j$ are fixed, and in

this case the scalar function like C_0^6 is proportional to $\frac{1}{m_{\tilde{g}}^2} \log \frac{m_S^2}{m_{\tilde{g}}^2} \left[1 + \frac{\hat{s}}{2m_{\tilde{g}}^2} \right]$ when $m_{\tilde{g}}^2 \gg \hat{s}$ (see Eq. (6.18,6.26)), thus the SUSY QCD correction goes like $\frac{1}{m_{\tilde{g}}} \log \frac{m_S^2}{m_{\tilde{g}}^2}$.

In the scenario, since \hat{s} can be up to the large collider beam energy squared s , therefore, not only the logarithmic dependence on the large mass parameter but also the large collider beam energies are responsible for the slow decoupling of the gluino, especially, at LHC, as shown in the figure. This is different from the previous studies in various decays [8–10].

(4) *Scenario D*: Only squark masses are of the same order (collectively denoted by m_S) and very large than other SUSY parameters and the electroweak scale

As shown in Fig. 5, the SUSY QCD also decouples. In this case, it decouples much faster than in *Scenario C* where only gluino mass gets large. This can be understood easily because in this case the couplings α_{ij} in the vertex $H^- \tilde{t}_i \tilde{b}_j$ and the mass of gluino are both fixed, so that the SUSY QCD correction goes like $\sim C_{11}^1 \rightarrow \frac{1}{m_S^2} \log \frac{m_S^2}{m_{\tilde{g}}^2}$.

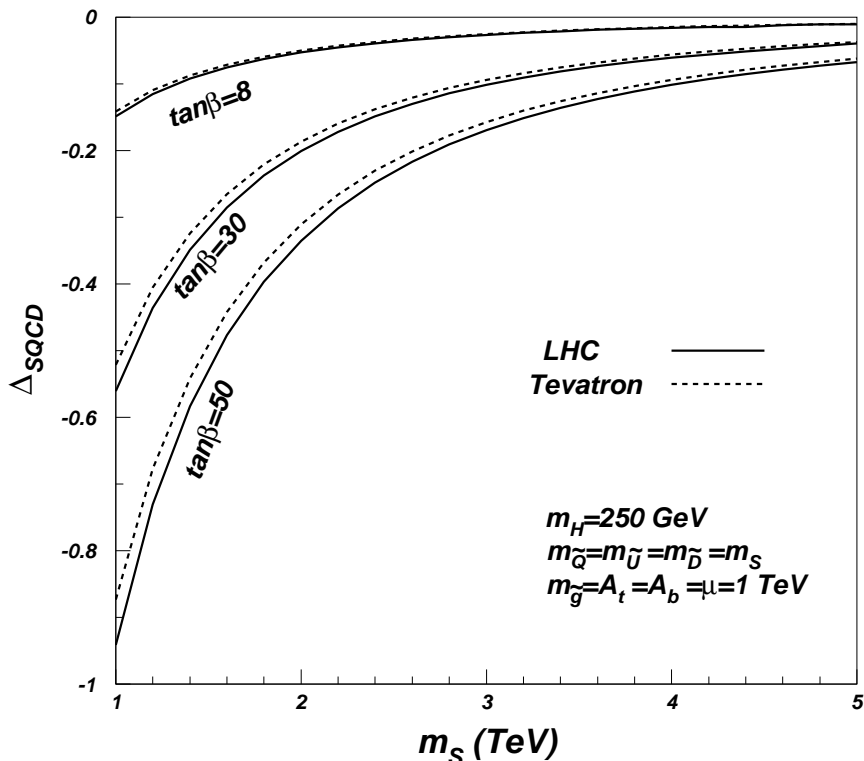


FIG. 5. Behavior of Δ_{SQCD} in the large squark masses limit with fixed $m_{\tilde{g}} = A_b = A_t = \mu = 1$ TeV and for different values of $\tan \beta$. The solid and dashed lines correspond to corrections at the Tevatron with $\sqrt{s} = 2$ TeV and at the LHC $\sqrt{s} = 14$ TeV, respectively.

Some remarks on the SUSY QCD correction to the process of $gb \rightarrow tH^\pm$ are in order:

1. From the above analysis we find that the fundamental reason for such non-decoupling behavior of SUSY QCD in the process $gb \rightarrow tH^\pm$ is that some couplings like $H^- \tilde{t}_i \tilde{b}_j$ are proportional to SUSY mass parameters. This is similar to the non-decoupling property of the heavy top quark in the SM, where the top quark Yukawa couplings are proportional to top quark mass.
2. The non-decoupling behavior shown in Fig. 3 is in agreement with previous studies of SUSY-QCD corrections in some decay process [8,9]. In particular, the correction Δ_{SQCD} shown in this figure as a function of the common scale m_S and $\tan \beta$ looks quite similar to the corresponding corrections in the partial decay width $\Gamma(H^+ \rightarrow t\bar{b})$, as given in Fig.2 of Ref. [8]. The same kind of similarities are also found between Fig.4 and Fig. 6 of Ref. [8], and between Fig.5 and Fig.7 of Ref. [8]. Although the processes are different, the fundamental reason for such non-decoupling behavior is the same.

3. From Figs. 3-5 one sees that the size of SUSY-QCD corrections can be quite large for large $\tan\beta$. Note that when one-loop effects are too large, higher-level loops must be also calculated. We refer the reader to Ref. [17] where some techniques of resummation for a better convergence are proposed.
4. As shown in Ref. [4], the genuine QCD corrections to this process is also sizable, which can enhance the production rate by 40% \sim 80% when charged Higgs mass and $\tan\beta$ vary in the range 180 \sim 1000 GeV and 2 \sim 50, respectively. It is clear that the SUSY-QCD correction evaluated in this work is comparable in size to the genuine QCD corrections. It is noticeable that the genuine QCD corrections are always positive whereas the SUSY-QCD corrections are negative in most SUSY parameter space.

V. CONCLUSIONS

In this work we have evaluated SUSY QCD radiative corrections to the $gb \rightarrow tH^\pm$ at Tevatron and LHC. We have found that in some parameter space the one-loop SUSY-QCD correction can be quite large and cannot be neglected. We have discussed in detail on the decoupling behavior of the corrections in the large SUSY mass limit, and found that with fixed gluino mass the one-loop SUSY QCD corrections decouple; while non-decoupling occurs when gluino mass and μ or A parameters both get large. The non-decoupling behavior of the SUSY-QCD corrections in the process $gb \rightarrow tH^-$ is similar to the ones found in the literatures for the Higgs particles and top quark decays. We pointed out that such non-decoupling behavior arises from the $H^- \tilde{t}_i \tilde{b}_j$ vertices which are proportional to SUSY mass parameters, as stated in some previous literatures [8–10]. Such large non-decoupling effects may play an important role in the indirect search for SUSY from the production of a top quark associated with a charged Higgs boson at Tevatron and LHC.

ACKNOWLEDGMENT

This work is supported in part by a grant of Chinese Academy of Science for Outstanding Young Scholars.

VI. APPENDIX A

Here we list the coefficients C^l , scalar functions $h_n^{(l)}$ and the vertex $V(H^- \tilde{t}_i \tilde{b}_j) = ig\alpha_{ij}/\sqrt{2}m_W$ ($i, j = 1, 2$) needed in our calculations.

- Coefficients C^l

$$\begin{aligned}
C^{V(s)} &= \frac{1}{\hat{s} - m_b^2}, C^{V(t)} = \frac{1}{\hat{t} - m_t^2}, \\
C^{s(s)} &= \frac{1}{(\hat{s} - m_b^2)^2}, C^{s(t)} = \frac{1}{(\hat{t} - m_t^2)^2}, C^{box} = 1.
\end{aligned} \tag{6.1}$$

- Scalar functions $h_n^{(l)}$

$$\begin{aligned}
h_1^{(l)} &= 4m_t\eta_t(2p_b \cdot k - p^{(l)} \cdot p_b) - 4m_b\eta_b(p^{(l)} \cdot p_t + p_t \cdot k), \\
h_3^{(l)} &= 2\eta_t(2p_b \cdot kp_b \cdot p_t - m_b^2 p_t \cdot k - 2p^{(l)} \cdot p_b p_b \cdot p_t) + 2m_b m_t \eta_b(p_b \cdot k - 2p^{(l)} \cdot p_b), \\
h_5^{(l)} &= 2\eta_t(m_t^2 p_b \cdot k - 2p^{(l)} \cdot p_t p_b \cdot p_t) + 2m_b m_t \eta_b(p_t \cdot k - 2p^{(l)} \cdot p_t), \\
h_7^{(l)} &= 4\eta_t(p^{(l)} \cdot p_b p_t \cdot k - p^{(l)} \cdot kp_b \cdot p_t - p_b \cdot kp^{(l)} \cdot p_t - 2p_b \cdot kp_t \cdot k) - 4m_b m_t \eta_b p^{(l)} \cdot k, \\
h_9^{(l)} &= 4m_t \eta_t p_b \cdot k(p_b \cdot k - p^{(l)} \cdot p_b) - 4m_b \eta_b p^{(l)} \cdot p_b p_t \cdot k, \\
h_{11}^{(l)} &= 4m_t \eta_t p_b \cdot k(p_t \cdot k - p^{(l)} \cdot p_t) - 4m_b \eta_b p_t \cdot kp^{(l)} \cdot p_t, \\
h_{2,4,6,8,10,12}^{(l)} &= h_{1,3,5,7,9,11}^{(l)}(\eta_b \leftrightarrow \eta_t),
\end{aligned} \tag{6.2}$$

where the index l represents the two channels s and t , and $p^{(s)} = p_b$, $p^{(t)} = p_t$.

- Couplings of $H^-\tilde{t}_i\tilde{b}_j$

The $H^-\tilde{t}_i\tilde{b}_j$ interaction terms can be parametrized as

$$\mathcal{L}_{H^-\tilde{t}_i\tilde{b}_j} = \frac{g}{\sqrt{2}m_W}\alpha_{ij} \quad (i, j = 1, 2), \quad (6.3)$$

where

$$\alpha_{ij} = R_{i1}^{t*}R_{j1}^b g_{LL} + R_{i2}^{t*}R_{j2}^b g_{RR} + R_{i1}^{t*}R_{j2}^b g_{LR} + R_{i2}^{t*}R_{j1}^b g_{RL} \quad (6.4)$$

with

$$\begin{aligned} g_{LL} &= -m_W^2 \sin 2\beta + m_b^2 \tan \beta + m_t^2 \cot \beta, \\ g_{RR} &= m_b m_t (\tan \beta + \cot \beta), \\ g_{LR} &= m_b (\mu + A_b \tan \beta), \\ g_{RL} &= m_t (\mu + A_t \cot \beta). \end{aligned} \quad (6.5)$$

APPENDIX B

The form factors F_n^l raise from the renormalized vertices and propagators of s-channel and t-channel, as well as box diagram given as following.

- The renormalized vertices of s-channel:

$$\begin{aligned} F_1^{V_1(s)} &= -3\eta_b \{ A_{bi}^1 m_{\tilde{g}} p_b \cdot k C_0^1 + A_{bi}^2 m_b [\hat{s} C_0^1 + m_b^2 (C_0^1 + 4C_{11}^1 + 2C_{21}^1) \\ &\quad + 2p_b \cdot k (C_{11}^1 + 2C_{12}^1 + 2C_{23}^1) - 2m_{\tilde{g}}^2 C_0^1 - 1 + 4C_{24}^1 + m_b p_b \cdot k (C_0^1 + C_{11}^1)] \} \\ &\quad + \frac{4}{3} A_{bi}^2 \eta_b m_b C_{24}^2 - \frac{16\pi^2}{g_s^2} \eta_t m_b (\delta Z_R^b - \delta Z_L^b), \\ F_3^{V_1(s)} &= \frac{2}{3} \eta_t \{ - [m_b^2 (C_{11}^1 + C_{21}^1) + p_b \cdot k (C_{12}^1 + C_{23}^1) + C_{24}^1] + A_{bi}^1 m_{\tilde{g}} m_b (C_0^1 + C_{11}^1) \\ &\quad + 2A_{bi}^2 [C_{24}^1 + p_b \cdot k (C_{12}^1 + C_{23}^1)] \} - 3\eta_t \{ [m_b^2 (C_0^2 + 2C_{11}^2 + C_{21}^2) + m_{\tilde{g}}^2 C_0^2 - 2C_{24}^2 + 1/2] \\ &\quad + 2A_{bi}^1 m_b m_{\tilde{g}} (C_0^2 + C_{11}^2) + 2A_{bi}^2 [m_b^2 (C_0^2 + 2C_{11}^2 + C_{21}^2) - m_{\tilde{g}}^2 C_0^2 - 1/2 + 2C_{24}^2] \} \\ &\quad + \frac{16\pi^2}{g_s^2} \eta_t 2\delta Z_R^b, \\ F_7^{V_1(s)} &= \frac{1}{3} \eta_t (C_{24}^1 - 2A_{bi}^2 C_{24}^1) - \frac{3}{2} \eta_t \{ m_b^2 (C_{21}^2 - C_0^2) + 2p_b \cdot k (C_{12}^2 + C_{23}^2) - m_{\tilde{g}}^2 C_0^2 + 2C_{24}^2 - 1/2 \\ &\quad - 2A_{bi}^1 m_b m_{\tilde{g}} C_0^2 - 2A_{bi}^2 [m_b^2 (C_0^2 + 2C_{11}^2 + C_{21}^2) + 2p_b \cdot k (C_{12}^2 + C_{23}^2) - m_{\tilde{g}}^2 C_0^2 - 1/2 + 2C_{24}^2] \} \\ &\quad + \frac{16\pi^2}{g_s^2} \eta_t \delta Z_R^b, \\ F_{2,4,8}^{V_1(s)} &= F_{1,3,7}^{V_1(s)} (\eta_t \leftrightarrow \eta_b, A_{bi}^2 \rightarrow -A_{bi}^2, R \leftrightarrow L), \\ F_9^{V_1(s)} &= \frac{1}{3} \eta_b [-m_b (C_{11}^1 + C_{21}^1) + A_{bi}^1 m_{\tilde{g}} (C_0^1 + C_{11}^1) + 2A_{bi}^2 m_b (2C_{12}^1 + 2C_{23}^1 - C_{11}^1 - C_{21}^1)] \\ &\quad - 3\eta_b [m_b (C_{11}^2 + C_{21}^2) + A_{bi}^1 m_{\tilde{g}} C_{11}^2 + 2A_{bi}^2 m_b (C_{11}^2 + C_{21}^2 - 2C_{12}^2 - 2C_{23}^2)], \\ F_{10}^{V_1(s)} &= F_9^{V_1(s)} (\eta_b \rightarrow \eta_t, A_{bi}^2 \rightarrow -A_{bi}^2), \end{aligned} \quad (6.6)$$

where the Feynman integrals are defined as $C^1 \equiv C(p_b, k, m_{\tilde{b}_i}, m_{\tilde{g}}, m_{\tilde{g}})$, $C^2 \equiv C(-p_b, -k, m_{\tilde{g}}, m_{\tilde{b}_i}, m_{\tilde{b}_i})$, $C^3 \equiv C(-p_t, -p_{H^-}, m_{\tilde{g}}, m_{\tilde{t}_i}, m_{\tilde{b}_j})$ and

$$\begin{aligned}
F_1^{V_2(s)} &= \frac{8}{3} \alpha_{ij} A_{ij}^{1R} p_b \cdot k C_{12}^3, \\
F_2^{V_2(s)} &= F_1^{V_2(s)} (R \rightarrow L), \\
F_3^{V_2(s)} &= \frac{8}{3} \alpha_{ij} [A_{ij}^{1L} m_b C_{12}^3 + A_{ij}^{1R} m_t (C_{11}^3 - C_{12}^3) - m_{\bar{g}} A_{ij}^{2L} C_0^3] - \frac{16\pi^2}{g_s^2} \eta_t \left[\delta Z_R^t + \delta Z_L^b + 2 \frac{\delta m_t}{m_t} \right], \\
F_7^{V_2(s)} &= -\frac{4}{3} \alpha_{ij} [A_{ij}^{1L} m_b C_{12}^3 + A_{ij}^{1R} m_t (C_{11}^3 - C_{12}^3) - A_{ij}^{2L} m_{\bar{g}} C_0^3] + \frac{16\pi^2}{g_s^2} \eta_t \left[\frac{1}{2} \delta Z_R^t + \frac{1}{2} \delta Z_L^b + \frac{\delta m_t}{m_t} \right], \\
F_{4,8}^{V_2(s)} &= F_{3,7}^{V_2(s)} \left(R \leftrightarrow L, \eta_t \rightarrow \eta_b, \frac{\delta m_t}{m_t} \rightarrow \frac{\delta m_b}{m_b} \right). \tag{6.7}
\end{aligned}$$

Here $A_{(t,b)i}^1 = (-1)^i \sin 2\theta_{t,b}$, $A_{(t,b)i}^2 = \frac{1}{2}(-1)^i \cos 2\theta_{t,b}$. A_{ij} are defined as $A_{ij}^{1L} = 2R_{i2}^t R_{j2}^b$, $A_{ij}^{1R} = 2R_{i1}^t R_{j1}^b$, $A_{ij}^{2L} = -2R_{i2}^t R_{j1}^b$ and $A_{ij}^{2R} = -2R_{i1}^t R_{j2}^b$.

- The renormalized vertices of t-channel:

$$\begin{aligned}
F_1^{V_1(t)} &= \frac{4}{3} A_{ti}^2 \eta_t m_t C_{24}^4 + 3\eta_t \{ m_t p_t \cdot k (C_0^5 + C_{11}^5) + A_{ti}^1 m_{\bar{g}} p_t \cdot k C_0^5 \\
&\quad - A_{ti}^2 m_t [\hat{t} C_0^5 + m_t^2 (C_0^5 + 4C_{11}^5 + 2C_{21}^5) - 2p_t \cdot k (C_{11}^5 + 2C_{12}^5 + 2C_{23}^5) - 2m_{\bar{g}}^2 C_0^5 - 1 + 4C_{24}^5] \} \\
&\quad - \frac{16\pi^2}{g_s^2} \eta_t m_t (\delta Z_R^t - \delta Z_L^t), \\
F_5^{V_1(t)} &= \frac{2}{3} \eta_t \{ - [m_t^2 (C_{11}^4 + C_{21}^4) - p_t \cdot k (C_{12}^4 + C_{23}^4) + C_{24}^4] + A_{ti}^1 m_{\bar{g}} m_t (C_0^4 + C_{11}^4) \\
&\quad + 2A_{ti}^2 [-C_{24}^4 + p_t \cdot k (C_{12}^4 + C_{23}^4)] \} - 3\eta_t \{ m_t^2 (C_0^5 + 2C_{11}^5 + C_{21}^5) + m_{\bar{g}}^2 C_0^5 - 2C_{24}^5 + 1/2 \\
&\quad + 2A_{ti}^1 m_t m_{\bar{g}} (C_0^5 + C_{11}^5) - 2A_{ti}^2 [m_t^2 (C_0^5 + 2C_{11}^5 + C_{21}^5) - m_{\bar{g}}^2 C_0^5 - 1/2 + 2C_{24}^5] \} \\
&\quad - \frac{16\pi^2}{g_s^2} \eta_t 2\delta Z_R^t, \\
F_7^{V_1(t)} &= \frac{1}{3} \eta_t (C_{24}^4 + 2A_{ti}^2 C_{24}^4) + \frac{3}{2} \eta_t \{ m_t^2 (C_0^5 - C_{21}^5) + 2p_t \cdot k (C_{12}^5 + C_{23}^5) + m_{\bar{g}}^2 C_0^5 - 2C_{24}^5 + 1/2 \\
&\quad + 2A_{ti}^1 m_t m_{\bar{g}} C_0^5 - 2A_{ti}^2 [m_t^2 (C_0^5 + 2C_{11}^5 + C_{21}^5) - 2p_t \cdot k (C_{12}^5 + C_{23}^5) - m_{\bar{g}}^2 C_0^5 - 1/2 + 2C_{24}^5] \} \\
&\quad + \frac{16\pi^2}{g_s^2} \eta_t \delta Z_R^t, \\
F_{2,6,8}^{V_1(t)} &= F_{1,5,7}^{V_1(t)} (\eta_t \rightarrow \eta_b, A_{ti}^2 \rightarrow -A_{ti}^2, R \leftrightarrow L), \\
F_{11}^{V_1(t)} &= \frac{1}{3} \eta_t [m_t (C_{11}^4 + C_{21}^4) - A_{ti}^1 m_{\bar{g}} (C_0^4 + C_{11}^4) - 2A_{ti}^2 m_t (2C_{12}^4 + 2C_{23}^4 - C_{11}^4 - C_{21}^4)] \\
&\quad + 3\eta_t [m_t (C_{11}^5 + C_{21}^5) + A_{ti}^1 m_{\bar{g}} C_{11}^5 + A_{ti}^2 2m_t (C_{11}^5 + C_{21}^5 - 2C_{12}^5 - 2C_{23}^5)], \\
F_{12}^{V_1(t)} &= F_{11}^{V_1(t)} (\eta_t \rightarrow \eta_b, A_{ti}^2 \rightarrow -A_{ti}^2), \tag{6.8}
\end{aligned}$$

where the Feynman integrals are defined as $C^4 \equiv C(-p_t, k, m_{\bar{g}}, m_{\bar{t}_i}, m_{\bar{t}_i})$, $C^5 \equiv C(-p_t, k, m_{\bar{t}_i}, m_{\bar{g}}, m_{\bar{g}})$, $C^6 \equiv C(-p_b, p_{H^-}, m_{\bar{g}}, m_{\bar{b}_j}, m_{\bar{t}_i})$ and

$$\begin{aligned}
F_1^{V_2(t)} &= -\frac{8}{3} \alpha_{ij} A_{ij}^{1R} p_t \cdot k C_{12}^6, \\
F_2^{V_2(t)} &= F_1^{V_2(t)} (R \rightarrow L), \\
F_5^{V_2(t)} &= \frac{8}{3} \alpha_{ij} [A_{ij}^{1L} m_b (C_{11}^6 - C_{12}^6) + A_{ij}^{1R} m_t C_{12}^6 - A_{ij}^{2L} m_{\bar{g}} C_0^6] - \frac{16\pi^2}{g_s^2} \eta_t \left[\delta Z_R^t + \delta Z_L^b + 2 \frac{\delta m_t}{m_t} \right], \\
F_7^{V_2(t)} &= -\frac{4}{3} \alpha_{ij} [A_{ij}^{1L} m_b (C_{11}^6 - C_{12}^6) + A_{ij}^{1R} m_t C_{12}^6 - A_{ij}^{2L} m_{\bar{g}} C_0^6] + \frac{16\pi^2}{g_s^2} \eta_t \left[\frac{1}{2} \delta Z_R^t + \frac{1}{2} \delta Z_L^b + \frac{\delta m_t}{m_t} \right], \\
F_{6,8}^{V_2(t)} &= F_{5,7}^{V_2(t)} \left(R \leftrightarrow L, \eta_t \rightarrow \eta_b, \frac{\delta m_t}{m_t} \rightarrow \frac{\delta m_b}{m_b} \right). \tag{6.9}
\end{aligned}$$

- The renormalized propagator of s-channel:

$$\begin{aligned}
F_1^{s(s)} &= \frac{16\pi^2}{g_s^2} \eta_b \left[2m_b p_b \cdot k (\hat{\Sigma}_L^b + \hat{\Sigma}_S^b) \right], \\
F_3^{s(s)} &= \frac{16\pi^2}{g_s^2} \eta_t \left[2 \left(\hat{s} \hat{\Sigma}_L^b + m_b^2 \hat{\Sigma}_R^b \right) + 4m_b^2 \hat{\Sigma}_S^b \right], \\
F_7^{s(s)} &= -\frac{16\pi^2}{g_s^2} \eta_t \left[\hat{s} \hat{\Sigma}_L^b + m_b^2 \hat{\Sigma}_R^b + 2m_b^2 \hat{\Sigma}_S^b \right], \\
F_{2,4,8}^{s(s)} &= F_{1,3,7}^{s(s)} (\eta_t \leftrightarrow \eta_b, R \leftrightarrow L).
\end{aligned} \tag{6.10}$$

- The renormalized propagator of t-channel:

$$\begin{aligned}
F_1^{s(t)} &= -\frac{16\pi^2}{g_s^2} \eta_t \left[2m_t p_t \cdot k (\hat{\Sigma}_L^t + \hat{\Sigma}_S^t) \right], \\
F_5^{s(t)} &= \frac{16\pi^2}{g_s^2} \eta_t \left[2 \left(\hat{t} \hat{\Sigma}_R^t + m_t^2 \hat{\Sigma}_L^t \right) + 4m_t^2 \hat{\Sigma}_S^t \right], \\
F_7^{s(t)} &= -\frac{16\pi^2}{g_s^2} \eta_t \left[\hat{t} \hat{\Sigma}_R^t + m_t^2 \hat{\Sigma}_L^t + 2m_t^2 \hat{\Sigma}_S^t \right], \\
F_{2,6,8}^{s(t)} &= F_{1,5,7}^{s(t)} (\eta_t \rightarrow \eta_b, R \leftrightarrow L).
\end{aligned} \tag{6.11}$$

- Box diagram contribution:

$$\begin{aligned}
F_1^{box} &= \frac{1}{3} \alpha_{ij} A_{ij}^{1R} \left\{ 9 \left[D_{27}^1 + \frac{1}{2} (m_t^2 D_{22}^1 + m_H^2 D_{23}^1) - p_t \cdot k D_{24}^1 + (p_t \cdot k - p_b \cdot k) D_{25}^1 \right. \right. \\
&\quad \left. \left. + (p_t \cdot p_b + p_t \cdot k - m_t^2) D_{26}^1 - p_t \cdot k (D_{12}^1 - D_{13}^1) - \frac{1}{2} m_{\bar{g}}^2 D_0^1 \right] - D_{27}^2 \right\}, \\
F_3^{Box} &= \frac{1}{3} \alpha_{ij} \left\{ -9 [A_{ij}^{1L} m_b D_{23}^1 + A_{ij}^{1R} m_t (D_{23}^1 - D_{26}^1) - A_{ij}^{2L} m_{\bar{g}} D_{13}^1] \right. \\
&\quad \left. + A_{ij}^{1L} m_b (D_{13}^2 - D_{11}^2 - D_{21}^2 - D_{23}^2 + 2D_{25}^2) - A_{ij}^{1R} m_t (D_{13}^2 + D_{25}^2 - D_{23}^2) \right. \\
&\quad \left. + A_{ij}^{2L} m_{\bar{g}} (D_0^2 + D_{11}^2 - D_{13}^2) \right\}, \\
F_5^{box} &= \frac{1}{3} \alpha_{ij} \left\{ 9 [A_{ij}^{1L} m_b (D_{23}^1 - D_{26}^1) - A_{ij}^{1R} m_t (D_{22}^1 + D_{23}^1 - 2D_{26}^1) + A_{ij}^{2L} m_{\bar{g}} (D_{12}^1 - D_{13}^1)] \right. \\
&\quad \left. + A_{ij}^{1L} m_b (D_{23}^2 - D_{25}^2) - A_{ij}^{1R} m_t D_{23}^2 + A_{ij}^{2L} m_{\bar{g}} D_{13}^2 \right\}, \\
F_7^{box} &= -\frac{3}{2} \alpha_{ij} [A_{ij}^{1L} m_b D_{13}^1 + A_{ij}^{1R} m_t (D_{12}^1 - D_{13}^1) - A_{ij}^{2L} m_{\bar{g}} D_0^1], \\
F_9^{box} &= \frac{1}{3} \alpha_{ij} A_{ij}^{1R} \left\{ -9 (D_{23}^1 - D_{25}^1) + D_{13}^2 - D_{12}^2 - D_{24}^2 - D_{23}^2 + D_{25}^2 + D_{26}^2 \right\}, \\
F_{11}^{box} &= \frac{1}{3} \alpha_{ij} A_{ij}^{1R} \left\{ 9 [D_{12}^1 - D_{13}^1 + D_{23}^1 + D_{24}^1 - D_{25}^1 - D_{26}^1] D_{23}^2 - D_{26}^2 \right\}, \\
F_{2,4,6,8,10,12}^{box} &= F_{1,3,5,7,9,11}^{box} (R \leftrightarrow L)
\end{aligned} \tag{6.12}$$

where four-point functions are defined as $D^1 \equiv D(k, -p_t, -p_{H^-}, m_{\bar{g}}, m_{\bar{g}}, m_{\bar{t}_i}, m_{\bar{b}_j})$, $D^2 \equiv D(-p_b, -k, p_{H^-}, m_{\bar{g}}, m_{\bar{b}_j}, m_{\bar{b}_j}, m_{\bar{t}_i})$. Note in the above formula we take the convention that repeated indices are summed over.

All other form factors F_n^l not listed above vanish. Note that the contributions from diagrams Fig. 1(i), 1(j) and 1(k) just give the renormalization constant δZ_2^g , which is canceled out by δg_s due to the renormalization condition in Eq. (2.4).

The renormalization constants appearing in the above form factors are given by

$$\delta Z_L^t = -\frac{g_s^2 C_F}{16\pi^2} \left\{ m_t \left[2m_t \frac{\partial B_1}{\partial p_t^2} - m_{\bar{g}} A_{ti}^1 \frac{\partial B_0}{\partial p_t^2} \right] \Big|_{p_t^2 = m_t^2} + (1 - 2A_{ti}^2) B_1 \right\} (p_t^2, m_{\bar{g}}^2, m_{\bar{t}_i}^2),$$

$$\begin{aligned}
\delta Z_L^b &= -\frac{g_s^2 C_F}{16\pi^2} \left\{ m_b \left[2m_b \frac{\partial B_1}{\partial p_b^2} - m_{\bar{g}} A_{bi}^1 \frac{\partial B_0}{\partial p_b^2} \right] \Big|_{p_b^2=m_b^2} + (1 - 2A_{bi}^2) B_1 \right\} (p_b^2, m_{\bar{g}}^2, m_{b_i}^2), \\
\delta Z_R^t &= \delta Z_L^t (A_{ti}^2 \rightarrow -A_{ti}^2), \\
\delta Z_R^b &= \delta Z_L^b (A_{bi}^2 \rightarrow -A_{bi}^2), \\
\delta m_t/m_t &= \frac{g_s^2 C_F}{16\pi^2} (B_1 - \frac{m_{\bar{g}}}{m_t} A_{ti}^1 B_0) (p_t^2, m_{\bar{g}}^2, m_{t_i}^2), \\
\delta m_b/m_b &= \frac{g_s^2 C_F}{16\pi^2} (B_1 - \frac{m_{\bar{g}}}{m_b} A_{bi}^1 B_0) (p_b^2, m_{\bar{g}}^2, m_{b_i}^2),
\end{aligned} \tag{6.13}$$

where the color factor $C_F = 4/3$. The renormalized self energy contributions from quarks as follows

$$\begin{aligned}
\hat{\Sigma}_S^t &= \frac{g_s^2 C_F}{16\pi^2} \frac{m_{\bar{g}}}{m_t} A_{ti}^1 \left[B_0 (m_t^2, m_{\bar{g}}^2, m_{t_i}^2) - B_0 (\hat{t}, m_{\bar{g}}^2, m_{t_i}^2) \right], \\
\hat{\Sigma}_S^b &= \frac{g_s^2 C_F}{16\pi^2} \frac{m_{\bar{g}}}{m_b} A_{bi}^1 \left[B_0 (m_b^2, m_{\bar{g}}^2, m_{b_i}^2) - B_0 (\hat{s}, m_{\bar{g}}^2, m_{b_i}^2) \right], \\
\hat{\Sigma}_L^t &= -\frac{g_s^2 C_F}{16\pi^2} (1 - 2A_{ti}^2) B_1 (\hat{t}, m_{\bar{g}}^2, m_{t_i}^2) - \delta Z_L^t, \\
\hat{\Sigma}_L^b &= -\frac{g_s^2 C_F}{16\pi^2} (1 - 2A_{bi}^2) B_1 (\hat{s}, m_{\bar{g}}^2, m_{b_i}^2) - \delta Z_L^b, \\
\hat{\Sigma}_R^t &= \hat{\Sigma}_L^t (A_{ti}^2 \rightarrow -A_{ti}^2), \\
\hat{\Sigma}_R^b &= \hat{\Sigma}_L^b (A_{bi}^2 \rightarrow -A_{bi}^2).
\end{aligned} \tag{6.14}$$

APPENDIX C

In this appendix we give the expansions of the scalar loop integrals in the asymptotic large mass limit. The definitions and conventions of the Feynman loop integral functions can be found in [18]. The integrals are performed in $4 - \epsilon$ dimension and the divergent contributions are regularized by $\Delta \equiv (2/\epsilon) - \gamma_E + \log(4\pi) - \log(m_h^2/\mu_0^2)$ with m_h being the corresponding mass of the heavy particle in the loops and μ_0 , the regularization scale.

Under the assumption of $m_h^2 = \max(m_k^2) \gg p_i \cdot p_j$ ($i, j = 1, 2; k = 1, 2, 3$), we consider special cases used in our calculations. For the two-point function $B_1(p^2, m_h^2, m_l^2)$, we obtain

$$B_1 = \frac{1}{2} \left[\Delta + \frac{3 - \delta}{2(1 - \delta)} + \frac{2\delta - \delta^2}{(1 - \delta)^2} \log \delta \right] + \mathcal{O} \left(\frac{p^2}{m_h^2} \right) \tag{6.15}$$

where $\delta = m_l^2/m_h^2$. Therefore, the asymptotic form can be expressed as

$$B_1 = \begin{cases} \frac{\Delta}{2} + \frac{p^2}{12m_h^2}, & \delta \rightarrow 1, \\ \frac{\Delta}{2} + \frac{3}{4} + \frac{p^2}{3m_h^2}, & \delta \rightarrow 0, \\ \frac{\Delta}{2} + \frac{1}{4} + \frac{p^2}{6m_h^2}, & \delta \rightarrow \infty. \end{cases} \tag{6.16}$$

Note in the case $\delta \rightarrow \infty$, m_h in Eq. (6.16) should be replaced by m_l .

For the three-point function $C_{(0,24)}(p_1, p_2, m_1^2, m_2^2, m_3^2)$ we expand them as follows:

- Case A: $m_h = m_1, m_l^2 = m_2^2 = m_3^2 \pm \Delta_m^2$

$$\begin{aligned}
C_0 &= \frac{1}{m_h^2} \left\{ \frac{1}{1 - \delta} + \frac{1}{(1 - \delta)^2} \ln \delta + \frac{p^2}{m_h^2} \left[\frac{\delta + 5}{4(1 - \delta)^3} + \frac{2\delta + 1}{2(1 - \delta)^4} \ln \delta \right] + \mathcal{O} \left(\frac{\Delta_m^2}{m_h^2} \right) + \mathcal{O} \left(\frac{p^4}{m_h^4} \right) \right\}, \\
C_{24} &= \Delta + \frac{3 - \delta}{8(1 - \delta)} + \frac{2\delta - \delta^2}{4(1 - \delta)^2} \ln \delta + \frac{p^2}{24m_h^2} \left[\frac{2 + 5\delta - \delta^2}{(1 - \delta)^3} + \frac{6\delta}{(1 - \delta)^4} \ln \delta \right] + \mathcal{O} \left(\frac{\Delta_m^2}{m_h^2} \right) + \mathcal{O} \left(\frac{p^4}{m_h^4} \right)
\end{aligned} \tag{6.17}$$

where $p = p_1 + p_2$. In asymptotic large mass limit we obtain

$$C_0 = \begin{cases} -\frac{1}{2m_h^2} \left[1 + \frac{p^2}{12m_h^2} + \mathcal{O}\left(\frac{\Delta_m^2}{m_h^2}\right) + \mathcal{O}\left(\frac{p^4}{m_h^4}\right) \right], & \delta \rightarrow 1, \\ \frac{1}{m_h^2} \ln \frac{m_l^2}{m_h^2} \left[1 + \frac{p^2}{2m_h^2} + \mathcal{O}\left(\frac{\Delta_m^2}{m_h^2}\right) + \mathcal{O}\left(\frac{p^4}{m_h^4}\right) \right], & \delta \rightarrow 0. \end{cases} \quad (6.18)$$

$$C_{24} = \begin{cases} \Delta + \frac{p^2}{48m_h^2} + \mathcal{O}\left(\frac{\Delta_m^2}{m_h^2}\right) + \mathcal{O}\left(\frac{p^4}{m_h^4}\right), & \delta \rightarrow 1, \\ \Delta + \frac{3}{8} + \frac{p^2}{12m_h^2} + \mathcal{O}\left(\frac{\Delta_m^2}{m_h^2}\right) + \mathcal{O}\left(\frac{p^4}{m_h^4}\right), & \delta \rightarrow 0. \end{cases} \quad (6.19)$$

- Case B: $m_l = m_1, m_h = m_2 = m_3$

$$C_0 = -\frac{1}{m_h^2} \left\{ \frac{1}{1-\delta} + \frac{\delta}{(1-\delta)^2} \ln \delta + \frac{p^2}{m_h^2} \left[\frac{1+5\delta}{4(1-\delta)^3} + \frac{\delta^2+2\delta}{2(1-\delta)^4} \ln \delta \right] + \mathcal{O}\left(\frac{p^4}{m_h^4}\right) \right\},$$

$$C_{24} = \Delta + \frac{1-3\delta}{8(1-\delta)} - \frac{\delta^2}{4(1-\delta)^2} \ln \delta + \frac{p^2}{24m_h^2} \left[\frac{1-5\delta-2\delta^2}{(1-\delta)^3} - \frac{6\delta^2}{(1-\delta)^4} \ln \delta \right] + \mathcal{O}\left(\frac{p^4}{m_h^4}\right). \quad (6.20)$$

The asymptotic form is given by

$$C_0 = \begin{cases} -\frac{1}{2m_h^2} \left[1 + \frac{p^2}{12m_h^2} + \mathcal{O}\left(\frac{p^4}{m_h^4}\right) \right], & \delta \rightarrow 1, \\ -\frac{1}{m_h^2} \left[1 + \frac{p^2}{4m_h^2} + \mathcal{O}\left(\frac{p^4}{m_h^4}\right) \right], & \delta \rightarrow 0, \end{cases} \quad (6.21)$$

$$C_{24} = \begin{cases} \Delta + \frac{p^2}{48m_h^2} + \mathcal{O}\left(\frac{p^4}{m_h^4}\right), & \delta \rightarrow 1, \\ \Delta + \frac{1}{8} + \frac{p^2}{24m_h^2} + \mathcal{O}\left(\frac{p^4}{m_h^4}\right), & \delta \rightarrow 0. \end{cases} \quad (6.22)$$

For the four-point functions $D_{0,1k}(p_1, p_2, p_3, m_1^2, m_2^2, m_3^2, m_4^2)$ with the assumption of $m_h^2 = \max(m_k^2) \gg p^2 = \max(p_i \cdot p_j)$ ($i, j = 1, 2, 3; k = 1, 2, 3, 4$), we consider two special cases used in our calculations

- Case A: $m_h = m_1, m_l = m_2$

$$D_0 = \frac{1}{m_h^2 m_l^2} \left\{ \frac{1+\delta}{2(1-\delta)^2} + \frac{\delta}{(1-\delta)^3} \ln \delta + \mathcal{O}\left(\frac{\Delta_m^2}{m_h^2}\right) + \mathcal{O}\left(\frac{p^2}{m_h^2}\right) \right\},$$

$$D_{11} = \frac{1}{m_h^2 m_l^2} \left\{ \frac{2+5\delta-\delta^2}{4(1-\delta)^3} + \frac{3\delta}{(1-\delta)^4} \ln \delta + \mathcal{O}\left(\frac{\Delta_m^2}{m_h^2}\right) + \mathcal{O}\left(\frac{p^2}{m_h^2}\right) \right\},$$

$$D_{12} = \frac{2}{3} D_{11}, \quad D_{13} = \frac{1}{3} D_{11} \quad (6.23)$$

where $\Delta_m^2 = \max(|m_2^2 - m_3^2|, |m_2^2 - m_4^2|, |m_3^2 - m_4^2|)$. In asymptotic large mass limit we obtain

$$D_{(0,11,12,13)} = \begin{cases} \left(\frac{1}{6}, \frac{1}{8}, \frac{1}{12}, \frac{1}{24}\right) \frac{1}{m_h^4} \left[1 + \mathcal{O}\left(\frac{p^2}{m_h^2}\right) \right], & \delta \rightarrow 1, \\ \left(\frac{1}{2}, \frac{1}{2}, \frac{1}{3}, \frac{1}{6}\right) \frac{1}{m_h^2 m_l^2} \left[1 + \mathcal{O}\left(\frac{p^2}{m_h^2}\right) \right], & \delta \rightarrow 0. \end{cases} \quad (6.24)$$

- Case B: $m_h = m_1 = m_2, m_l^2 = m_3^2 = m_4^2 \pm \Delta_m^2$

$$D_0 = -\frac{1}{m_h^4} \left\{ \frac{2}{(1-\delta)^2} + \frac{1+\delta}{(1-\delta)^3} \ln \delta + \mathcal{O}\left(\frac{\Delta_m^2}{m_h^2}\right) + \mathcal{O}\left(\frac{p^2}{m_h^2}\right) \right\},$$

$$D_{11} = \frac{1}{m_h^4} \left\{ \frac{9+3\delta}{4(1-\delta)^3} + \frac{\delta^2-2\delta-2}{2(1-\delta)^4} \ln \delta + \mathcal{O}\left(\frac{\Delta_m^2}{m_h^2}\right) + \mathcal{O}\left(\frac{p^2}{m_h^2}\right) \right\},$$

$$D_{12} = -\frac{1}{m_h^4} \left\{ \frac{5+\delta}{2(1-\delta)^3} + \frac{1+2\delta}{(1-\delta)^4} \ln \delta + \mathcal{O}\left(\frac{\Delta_m^2}{m_h^2}\right) + \mathcal{O}\left(\frac{p^2}{m_h^2}\right) \right\},$$

$$D_{13} = \frac{1}{2} D_{12}. \quad (6.25)$$

In asymptotic large mass limit we obtain

$$D_{(0,11,12,13)} = \begin{cases} \left(\frac{1}{6}, \frac{1}{8}, \frac{1}{12}, \frac{1}{24}\right) \frac{1}{m_h^4} \left[1 + \mathcal{O}\left(\frac{\Delta^2}{m_h^2}\right) + \mathcal{O}\left(\frac{p^2}{m_h^2}\right)\right], & \delta \rightarrow 1, \\ (-1, -1, -1, -\frac{1}{2}) \frac{1}{m_h^4} \ln \frac{m_i^2}{m_h^2} \left[1 + \mathcal{O}\left(\frac{\Delta^2}{m_h^2}\right) + \mathcal{O}\left(\frac{p^2}{m_h^2}\right)\right], & \delta \rightarrow 0. \end{cases} \quad (6.26)$$

- [1] For a review, see, e.g., H. E. Haber, G. L. Kane, Phys. Rept. **117**, 75 (1985).
- [2] C. S. Li and J. M. Yang, Phys. Lett. B **315**, 367 (1993); C. S. Li, B. Q. Hu and J. M. Yang, D **47**, 2865 (1993). J. M. Yang, C. S. Li and B. Q. Hu, D **47**, 2872 (1993); J. A. Coarasa *et al.*, Eur. Phys. J. C **2**, 373 (1998).
- [3] F. Borzumati, J.-L. Kneur and N. Polonsky, Phys. Rev. D **60**, 115011 (1999); L. G. Jin, C. S. Li, R. J. Oakes and S.-H. Zhu, Phys. Rev. **D62**, 053008 (2000);
- [4] S.-H. Zhu, hep-ph/0112109.
- [5] A. C. Bawa, C. S. Kim and A. D. Martion, Z. Phys. **C 47**, 75 (1990); V. Barger, R. J. Phillips and D. P. Roy, Phys. Lett. **B324**, 236 (1994); S. Moretti and K. Odagiri, Phys. Rev. **D 55**, 5627 (1997).
- [6] J. Guasch, R. A. Jimenez and J. Sola, Phys. Lett. **B360**, 47 (1995); R. Jimenez and J. Sola, Phys. Lett. **B389**, 53 (1996); J. A. Coarasa and R. A. Jimenez and J. Sola, Phys. Lett. **B389**, 312 (1996).
- [7] For instance, see M. Carena, S. Mrenna and C. E. M. Wagner, Phys. Rev. **D60**, 075010 (1999), *ibid* **D62**, 055008 (2000); A. Belyaev, D. Garcia, J. Guasch and J. Sola, Phys. Rev. **D65**, 031701 (2002); A. Curiel *et al.*, Phys. Rev **D65**, 075006 (2002); R. A. Alanakyan and V. Grabski, hep-ph/9711436.
- [8] H. E. Haber, *et al.*, Phys. Rev. **D 63**, 055004 (2001).
- [9] M. J. Herrero, S. Peñaranda and D. Temes, Phys. Rev. **D64**, 115003 (2001).
- [10] A. Dobado and M. J. Herrero and D. Temes, Phys. Rev. **D65**, 075023(2002).
- [11] T. Appelquist and J. Carazzone, Phys. Rev. **D11**, 2856 (1975).
- [12] H. L. Lai, *et al.* (CTEQ collaboration), Eur. Phys. J. **C12**, 375 (2000).
- [13] J. F. Gunion and H. E. Harber, Nucl. Phys. **B272**, 1 (1986).
- [14] A. Djouadi, J. Kalinowski and M. Spira, Comp. Phys. Commun. **108**, 56 (1998).
- [15] H. N Brown, *et al.*, Mu g-2 Collaboration, Phys. Rev. Lett. **86**, 2227 (2001).
- [16] Particle Physics Group. Eur. Phys. J. **C15**, 274 (2000).
- [17] M. Carena, D. Garcia, U. Nierste and C. E. Wagner, Nucl. Phys. B **577** (2000) 88; H. Eberl *et al.*, Phys. Rev. D **62** (2000) 055006.
- [18] G. 't Hooft and M. Veltman, Nucl. Phys. **B153**, 365 (1979); G. Passarino and M. Veltman, Nucl. Phys. **B160**, 151 (1979).